Supporting Information

Near-Field Electrospinning for Three-Dimensional Stacked Nanoarchitectures with High Aspect Ratios

Yang-Seok Park,[1,2,+] *Junyoung Kim,*[1,2,+] *Jung Min Oh,*[1,2,†] *Seungyoung Park,*[3] *Seungse Cho,*[3] *Hyunhyub Ko,*[3] *Yoon-Kyoung Cho*[1,2,3]*

[1]Department of Biomedical Engineering, School of Life Sciences, Ulsan National Institute of Science and Technology (UNIST), Ulsan 44919, Republic of Korea

[2]Center for Soft and Living Matter, Institute for Basic Science (IBS), Ulsan 44919, Republic of Korea

[3]School of Energy and Chemical Engineering, Ulsan National Institute of Science and Technology (UNIST), Ulsan 44919, Republic of Korea

*To whom correspondence should be addressed: ykcho@unist.ac.kr.

The PDF file includes:

- Detailed description of experimental methods
- Supporting information video S1-S2
- Supporting information figures S1 – S9
- Supporting information table S1-S4

Numerical analysis of electrodynamics. Finite element method (FEM) simulations were performed using a software (COMSOL Multiphysics 5.1) to quantitatively test the effect of the salt on the electrohydrodynamics and fiber deposition in near-field electrospinning. The intensity and distribution of electric field and potential were calculated using "Electric Current" module in COMSOL. The geometric dimensions and material properties in simulations were identical to those of the experimental electrospinning setup. The voltage applied to the printing nozzle was 900 V and the substrate was grounded (**Figure 1B**). The medium between the printing polymer and the collector was set to air. The humidity of the air phase was not considered for simplicity. The electric properties of the various materials in this simulation are described in **Table S1**.

Preparation of solutions for 3D printing of nanofibrous architectures. 0.1–1 wt% of NaCl and 10 wt% of PEO was dissolved in DI water in order. During the dilution of PEO, the mixture was stirred for 24 h using a magnetic stir bar. Parameters of the prepared solution are shown in **Table S2**.

3D printing of nanofibrous architectures. First, temperature and humidity were fixed at 24 °C and 40 RH% using an air conditioner, a dehumidifier, and a humidifier controlled by LabVIEW. For the 3D printing, Si wafer substrates were prepared, and each was coated with a Cr (10 nm)/Au

(50 nm) layer by e-beam evaporation. The substrate was attached on the X–Y motion stage using double-sided tape. Subsequently, the prepared polymer solution was dispensed using a syringe pump so that a droplet with a size of 200 μm was formed at the tip of the blunt 27-gauge stainless-steel needle. Before spinning the nanofibers, the distance from the droplet and the substrate was fixed to 1 mm. Subsequently, a voltage of 900 V was applied to the stainless needle, and the polymer droplet was poked by a tungsten probe to initiate the nanofiber spinning process. During the spinning of the nanofibers, the x–y motion stage was controlled by a G-code to collect and pattern the nanofiber into desired designs at the speed of 400 mm/s. To create 3D nanofibrous architectures and to control their heights, the nanofibers were stacked in multiple layers by repeating the G-code-designed motion (**Figure S3**). For the preparation of transparent electrodes, 10 parallel alignment patterns with a length of 2 cm were printed in this study using multiple layers (20–100 layers).

Preparation of transparent electrodes. 3D printed nanofibrous architectures on the substrates were placed in a DC sputter for Ag deposition. Sputtering was conducted using 400 W for 120 s to deposit Ag at a thickness of 100 nm. After the Ag deposition, the samples were placed under vacuum with (tridecafluoro-1,1,2,2-tetrahydrooctyl)-1-trichlorosilane for 30 min to make it anti-adhesive. Subsequently, h–PDMS was prepared as follows: (1) A mixture of vinylmethylsiloxane/dimethylsiloxane (3.4 g), a solution of a platinum divinyltetramethyl-disiloxane complex in xylene (18 μL), and 2,4,6,8-tetramethyltetravinylcyclotetrasiloxane (20 μL) was prepared and degassed for 1 min in a vacuum chamber. (2) Methylhydrosiloxane (1 g) was added to the degassed mixture to produce h–PDMS. This h–PDMS was then coated by a spincoater at 1000 revolutions per minute (rpm) for 30 s. The h–PDMS coated sample was partially cured at

40 °C for 10 min. On the top of the sample, s–PDMS (5:1 ratio of base material and curing agent) was poured and cured at 40 °C overnight. After curing, the PDMS layer which was embedded with 3D Ag architectures was gently detached from the substrate. Only 3D Ag architectures become detached and were embedded in the PDMS layer owing to their high-aspect ratios.

Measurement of transmittance. Transmittance spectra of the transparent electrodes in visible wavelengths were obtained with the use of ultraviolet visible (UV-vis) microspectrophotometer (20/20 PV, Craic Technologies). The microscope stage was moved manually to measure the transmittance spectra of the position where the 3D Ag architecture was embedded in the PDMS. The transmittance values are obtained compared to the bare PDMS (used as a reference).

Electrical characterization. To characterize the electrical properties of the transparent electrode, two Au contact pads were formed at the opposite poles using sputtering. Two sharp probes were then gently contacted on the pads. Through the probes, the resistances and I–V characteristics of the transparent electrodes were measured by a DC voltage sweeping mode (-4 V–4 V, 0.1 V step) with an electrical characterization system (4200-SCS, Keithley).

Supporting information video S1 Effect of salt concentration on 3D printing of nanofibers

Supporting information video S2 Electrostatic attraction between deposited fibers and polymer solution

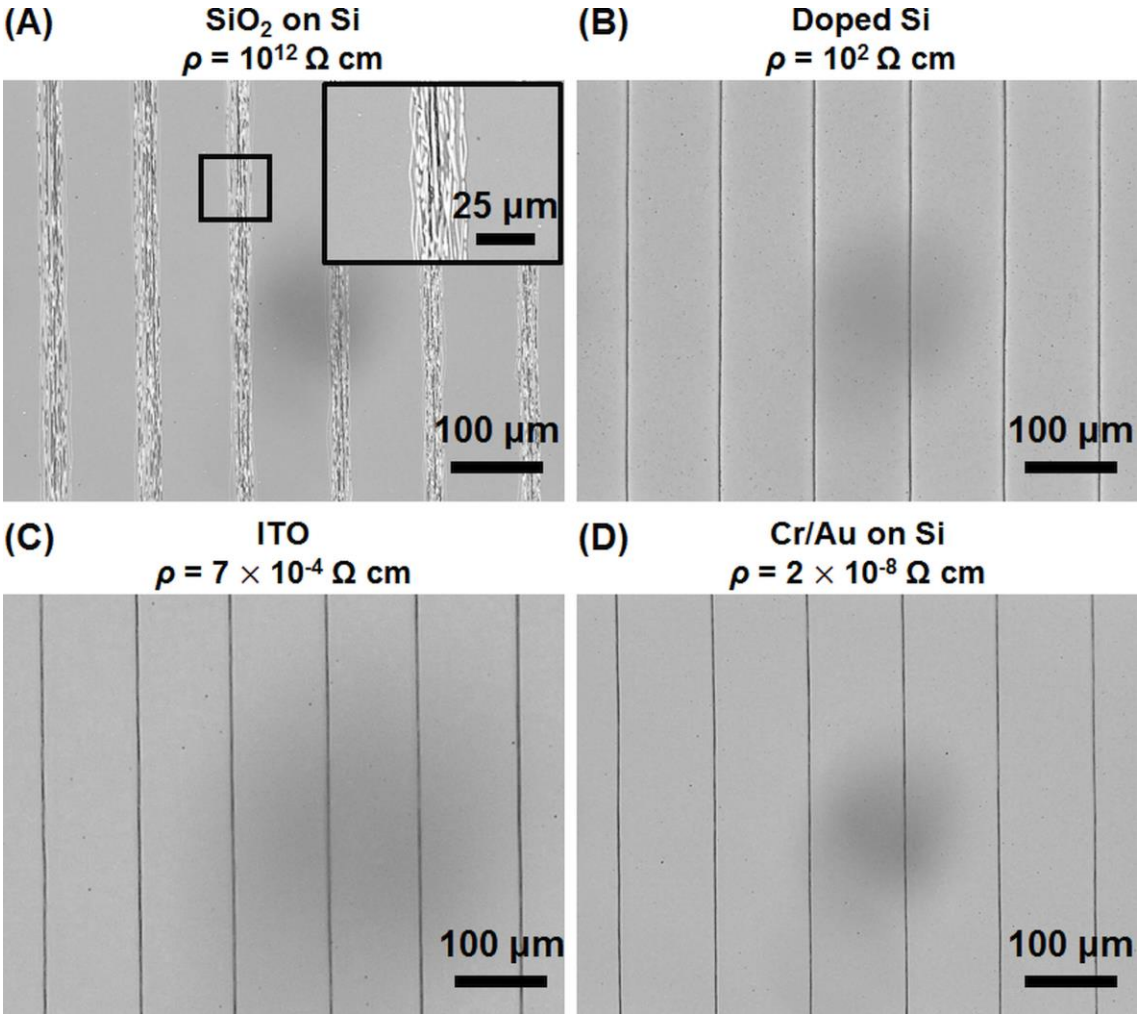

Figure S1. Optical image showing the significance of grounding on 3D nanoprinting based on the use of different types of substrates. (A) Insulating material (SiO_2) deposited on Si wafer was used as a substrate. Misaligned, nonstacked nanofibers were obtained. (B–D) Conducting materials (doped Si wafer, ITO (indium tin oxide) coated glass, Cr/Au) were also tested for 3D stacking. Precise construction of printed 3D nano-architectures was achieved for all the conducting materials.

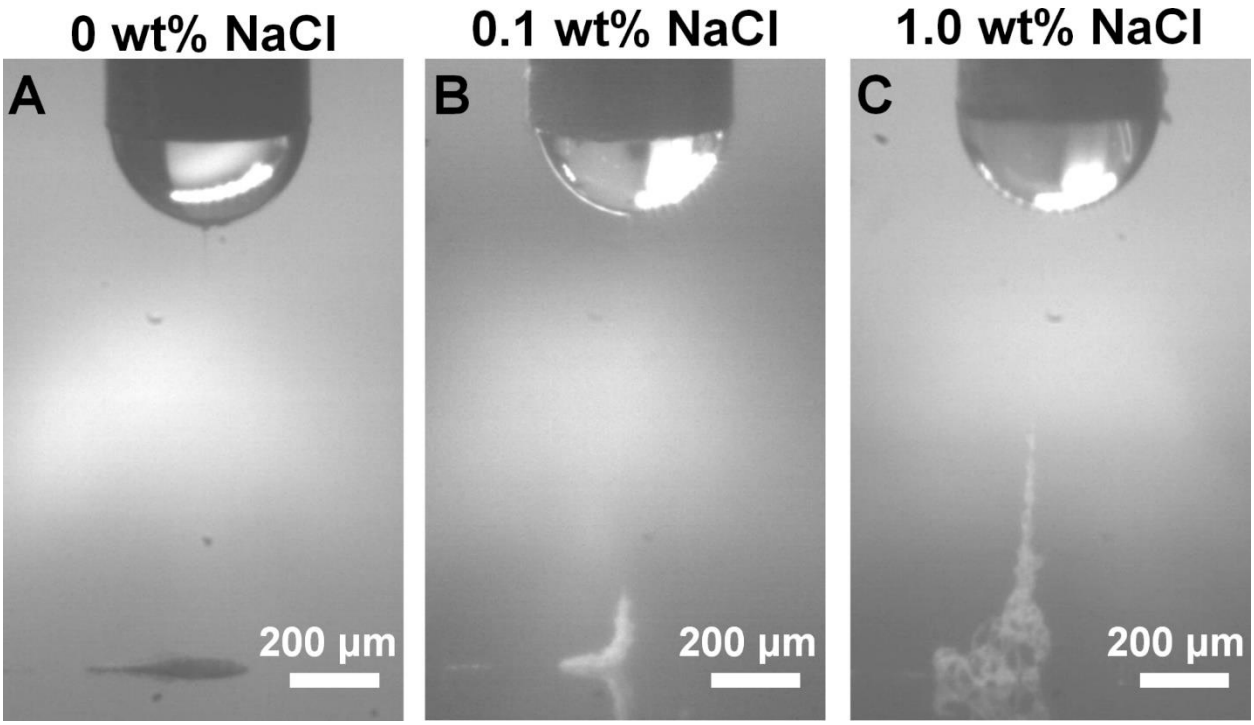

Figure S2. Effects of NaCl concentration in the PEO solution (10 wt%) on the electrostatic attraction among fibers using the 3D nanoprinting technique. (A–C) Charged-coupled device (CCD) camera images during NFES without stage motion. Shown are jetted nanofibers from polymer droplets in the presence of an electric field and deposited nanofibers on the Au deposited substrate (without x–y stage motion). The NaCl concentrations in the polymer solution are (A) 0 wt%, (B) 0.1 wt%, and (C) 1 wt%.

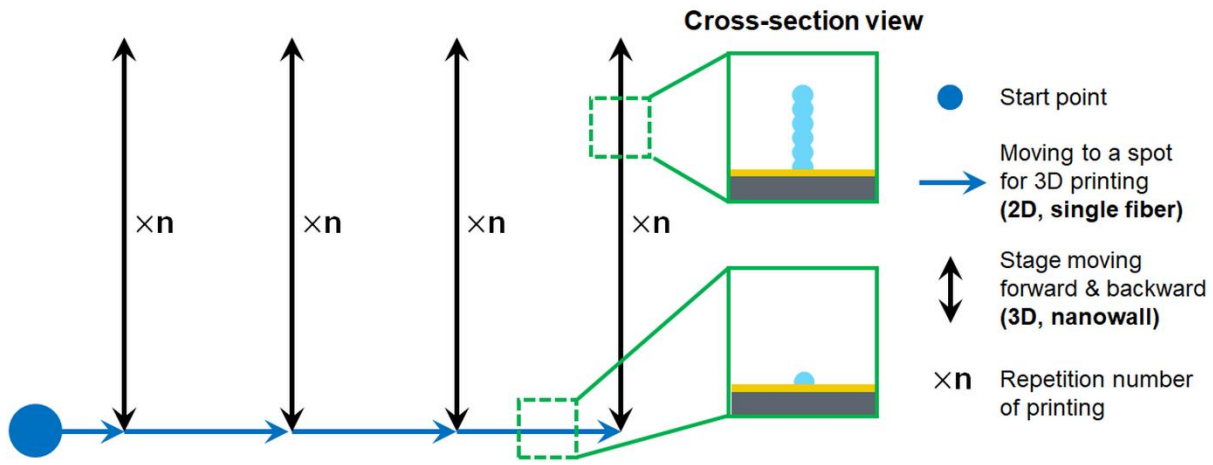

Figure S3. Motion design for the collection of nanofibers on a substrate for the 3D printing of nanowalls.

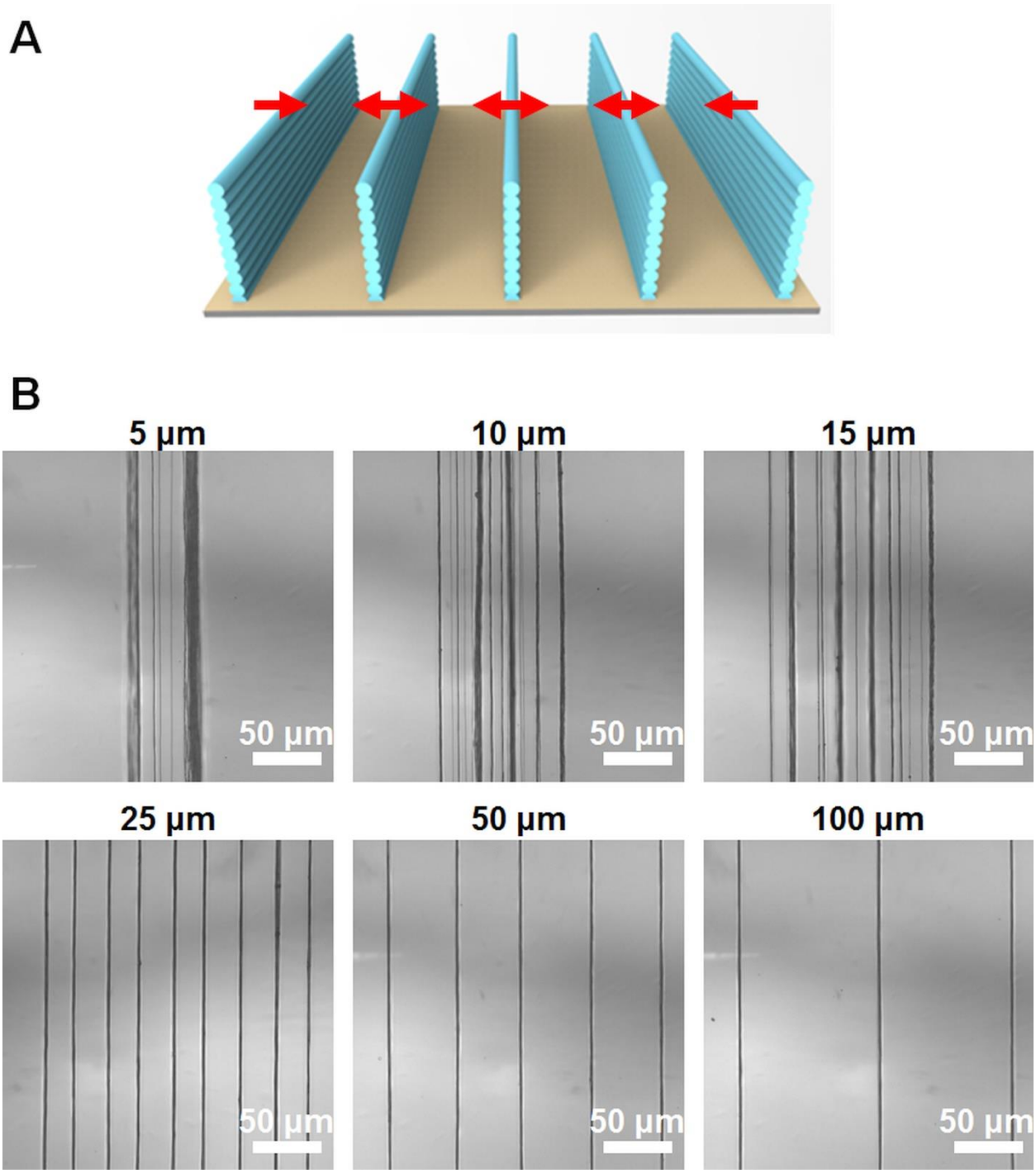

Figure S4. Optical images of 3D printed nanowall arrays with pitches ranging from 5 µm to 100 µm, when PEO with 1.0 wt% NaCl was used. The pitch was controllable down to 25 µm; however, when the pitch was decreased further, the fibers were misaligned and failed to stack orderly.

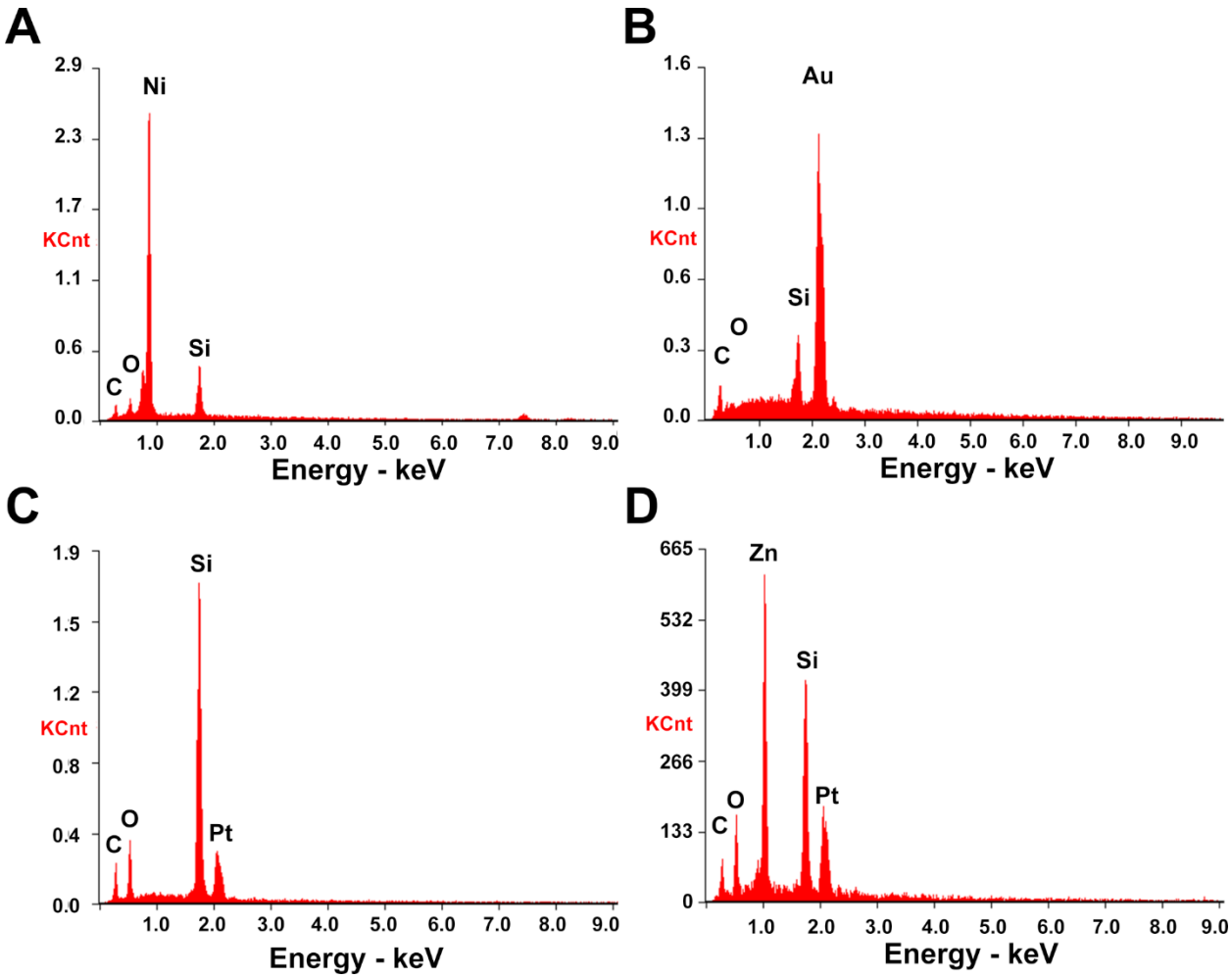

Figure S5. Energy-dispersive spectral (EDS) patterns of 3D nano-architectures coated with various functional materials, including (A) Ni, (B) Au, (C) SiO_2, and (D) ZnO, as shown in the main text. Structures coated with different materials are distinctly differentiated with distinct EDS peaks that represent the constituent materials.

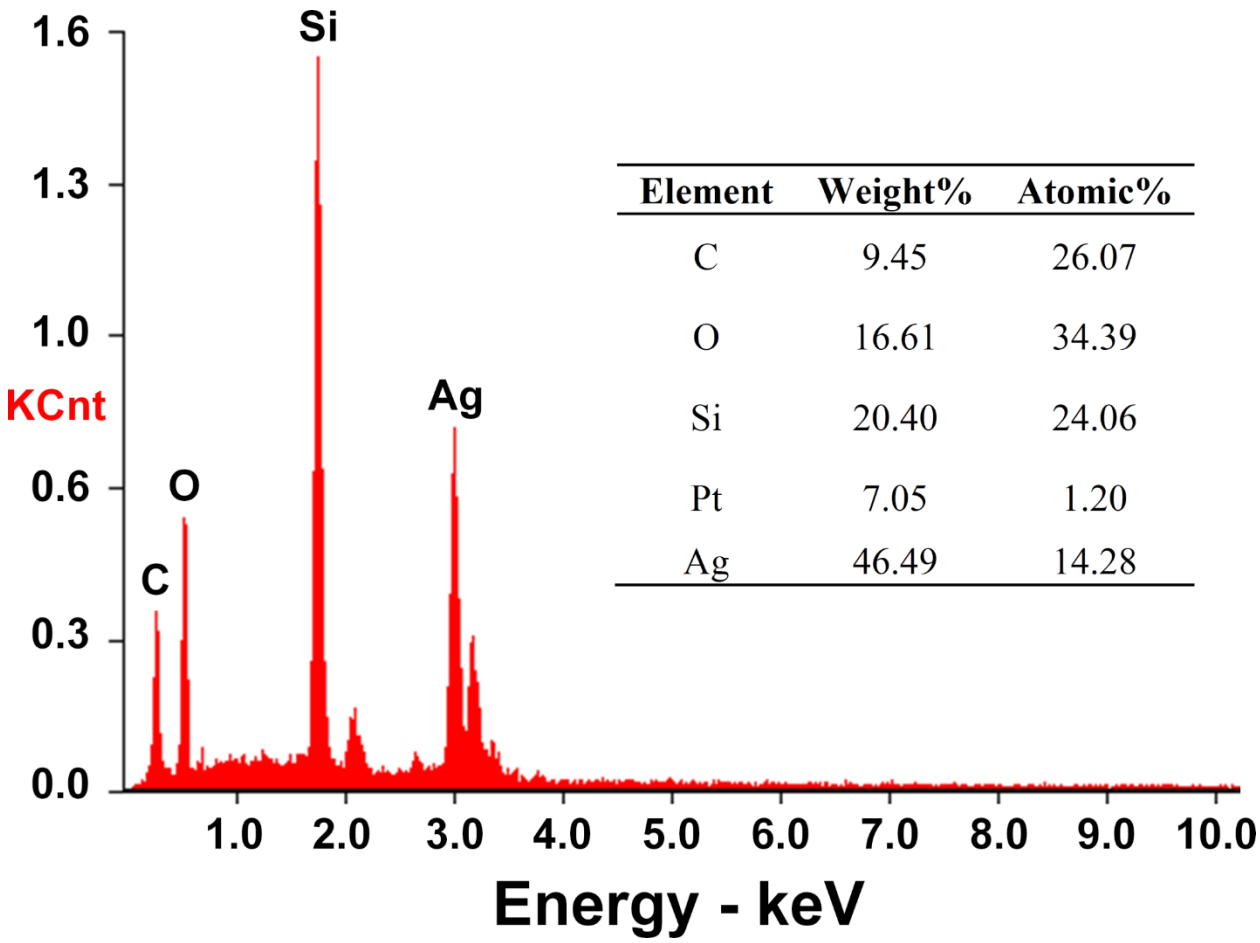

Element	Weight%	Atomic%
C	9.45	26.07
O	16.61	34.39
Si	20.40	24.06
Pt	7.05	1.20
Ag	46.49	14.28

Figure S6. EDS patterns of 3D Ag nanowire embedded in the PDMS. C, O, Si, originate from PDMS, and Pt is observed owing to the sputtering conducted for SEM imaging. Ag originates from the Ag 3D nanowire embedded in the PDMS.

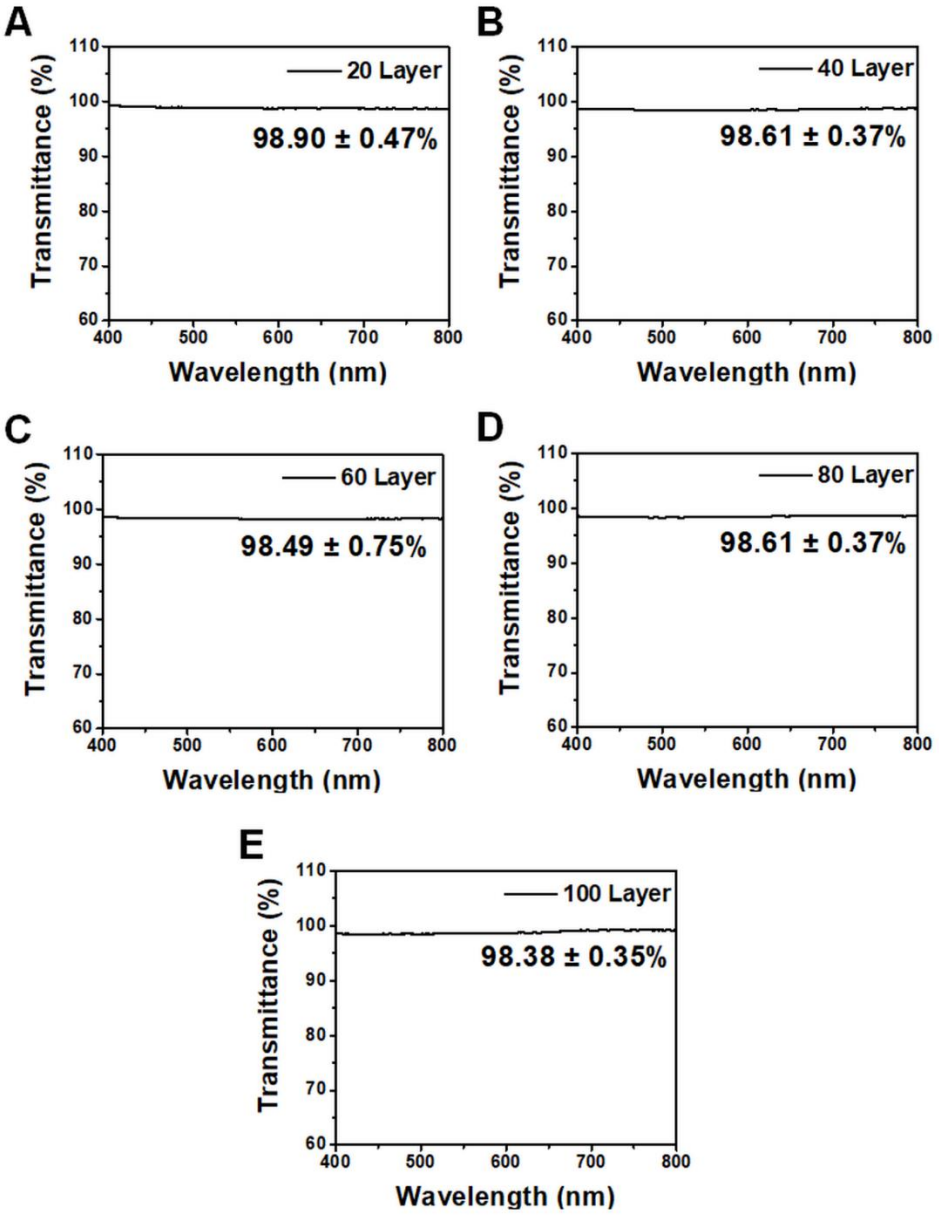

Figure S7. (A–F) Transmittances of the transparent electrodes in the visible wavelength range. Transmittance spectrum of a conductive PDMS film embedded with 3D Ag nanowires with various numbers of layers, including (A) 20, (B) 40, (C) 60, (D) 80, and (E) 100 layers. In this case, the transmittance value does not include the transmittance of the substrate (bare PDMS is used as a reference.).

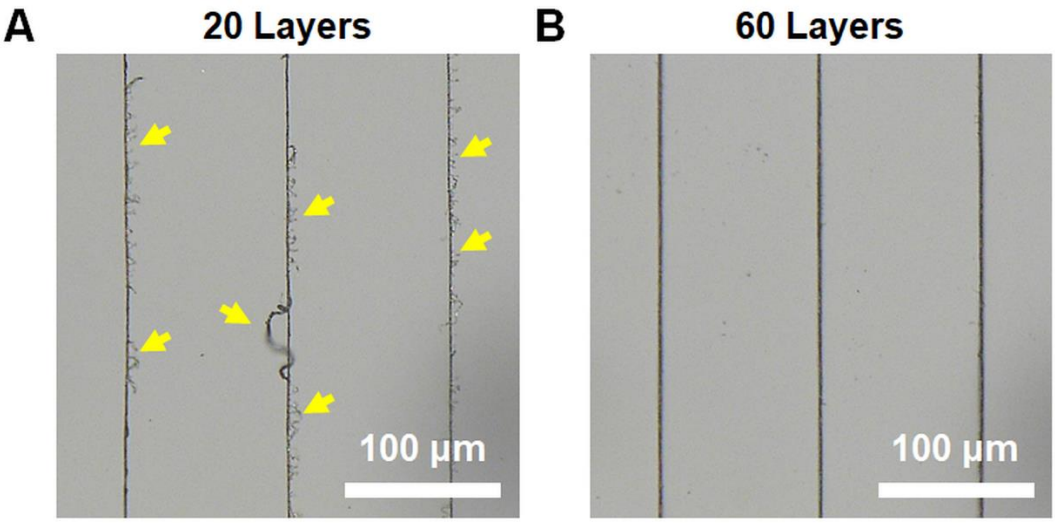

Figure S8. Quality of transparent electrodes depending on the number of 3D printed layers. (A, B) PDMS transparent electrode embedded with 3D Ag nanowires. (A) 3D Ag nanowires with a low-aspect ratio (20 layers) can peel off from the PDMS layer. (B) 3D Ag nanowires with a high-aspect ratio (60 layers) are stably embedded in the PDMS layer.

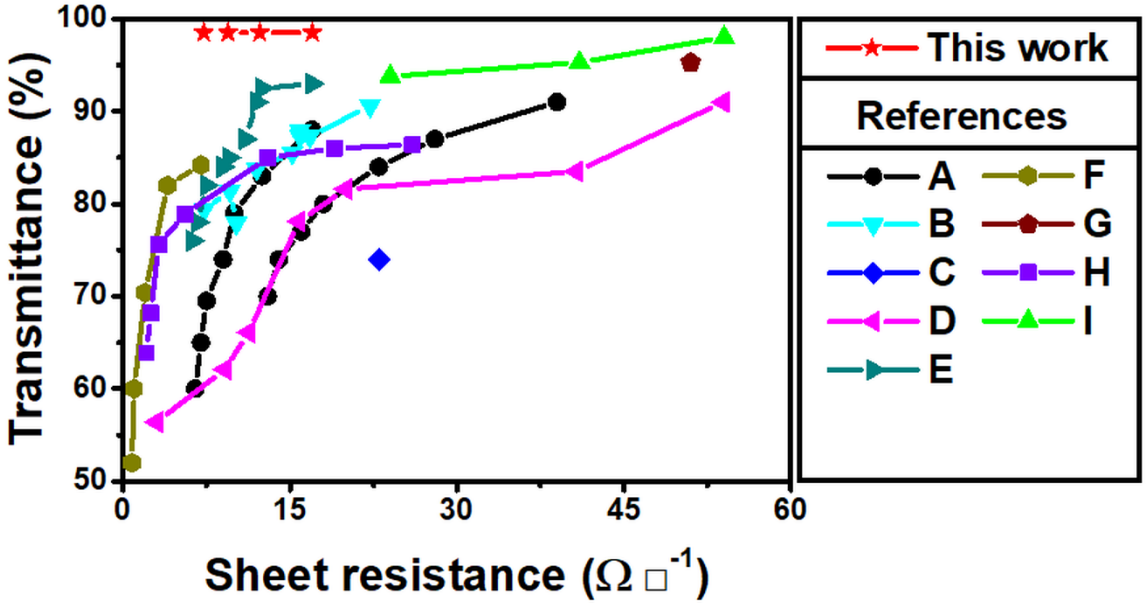

Legend	Sheet resistance (Ω □$^{-1}$)	Transmittance (%)	Max. aspect ratio of Ag electrodes	Reference
A	6.5	91	< 1	[1]
B	30	85	< 1	[2]
C	23	74	< 1	[3]
D	19	83	< 1	[4]
E	17	93	< 1	[5]
F	1 7	60 84	< 1	[6]
G	51	95	< 1	[7]
H	13	85	< 1	[8]
I	58	98	~7	[9]
This work	**17** **12** **9** **7**	**98.5**	**4–48**	**NOTE:** **Trade-off between resistance and transmittance is avoided.**

Figure S9. Variation of visible transmittance of transmittance electrodes (without substrates) as a function of sheet resistance. The chosen references from A to I show the performances of the Ag nanowires and printed Ag meshes fabricated by other techniques for comparison on.[1–9]

Table S1. Electric parameters of materials in numerical simulation

Materials	*Dielectric constant*	*Conductivity (S/m)*
PEO (Liquid)	80 [10]	0.58×10^{-1} ‡
PEO with NaCl (Liquid)	80 [10]	14.0×10^{-1} ‡
PEO (Polymer)	5 [11]	1.00×10^{-12} [12]
PEO with NaCl (Polymer)	250 [13]	1.00×10^{-5} [13]
Conductive substrate	1000	1.42×10^{5} ‡
Insulator	4.2	1.00×10^{-10} ‡
Air	1	1.00×10^{-9}

‡ This value is experimentally measured.

Table S2. Parameters of 10 wt% PEO solution with different concentration of NaCl

Concentration of NaCl in PEO solution (wt%)	*Viscosity (cP)*	*Surface tension (mN/m)*	*Conductivity (mS/cm)*
0.00	398 ± 44	48.9 ± 3.9	0.58
0.10	383 ± 24	50.5 ± 1.3	2.17
0.25	385 ± 33	52.1 ± 1.2	3.89
0.50	392 ± 38	51.3 ± 1.0	7.79
1.00	394 ± 45	50.4 ± 0.8	14.00

Table S3. Resistivity of the Ag nanowire in transparent electrodes.

Layers #	**Width (nm)**	**Height (μm)**	**Length (m)**	**Area‡× 10 lines (m^2)**	**Resistance (experiment) (Ω)**	**Resistivity (Ω m)**	**Sheet resistance¥ ($\Omega\ \square^{-1}$)**
40	200	4	0.02	8.0×10^{-12}	756	3×10^{-7}	17
60		6		1.2×10^{-11}	546	3×10^{-7}	12
80		8		1.6×10^{-11}	419	3×10^{-7}	9
100		10		2.0×10^{-11}	323	3×10^{-7}	7

[‡]The average resistivity of the Ag nanowires embedded in the transparent electrode is 3×10^{-7} Ω m. This value is highly comparable to the resistivity of recently studied 3D Ag structures, which is also 3×10^{-7} Ω m.[14] The 3D Ag structure in this reference has height of 37 μm and a diameter of 1.7 μm.

[¥]Sheet resistance value is calculated by considering the resistance of electrodes, length, and width of the area where the patterned 3D Ag nanowires are located (length = 2 cm, width = 50 μm, gap distance × 9 gaps between 10 patterns = 450 μm).

Table S4. Comparison with other NFES techniques used to build self-aligned and stacked 3D structures via layer-by-layer printing by design

Scale	*Diameter of printed fibers*	*Shape of 3D assembly demonstrated*	*On-demand design*	*Strategy*	*Ink*	*Substrate*	*Driving Voltage (kV)*	*Ref.*
Nano	92 ± 3 nm – 239 ± 30 nm	◆ Self-aligned, high aspect-ratio, 3D structure with controlled height ◆ Nanoscale straight walls, curved walls, grids, bridges	Yes	Addition of salt in polymer	PEO[1]	Conductive (Au, ITO, Si wafer)	0.9	This work
	180 nm	◆ Nanowalls which shape dictated by the pre-designed pattern of the electrodes	No	Patterned Pt electrode	PEO	Pt patterned on glass	1.5	[15]
	470 nm	◆ Free-standing hollow pottery	No	sharp electrode tip positioned underneath glass substrate.	PEO	sharp electrode tip positioned underneath glass substrate.	NA	[16]
	817 ± 165 nm	◆ Grids	Yes	Heater to melt polymers	PCL[2] melt	Al plate	2.9	[17]
Micro	20 ± 1.5 μm	◆ Grids	Yes	Heater to melt polymers & adjustment of voltage for constant electric field	PCL melt	Al plate	7 – 9	[18]
	2 – 10 μm	◆ Grids, walls, hollow cylinders, 3D logos	Yes	Enhanced local charge transfer between the deposited fiber and ground plate	PVDF[3]	Paper on the grounded conducting plate	1.5	[19]
	6 – 50 μm	◆ Grids	Yes	Enhanced focusing of electric field using electrostatic lens	PLGA[4]	Stainless-steel plate, Al foil, or Si wafer	16	[20]
	19 – 88 μm	◆ Grids	Yes	Heater to melt polymers with high viscosity for stable jetting	PCL	Al plate	8 – 10	[21]
	27 – 71 μm	◆ Straight wall, Curved features	Yes	Heater to melt polymers with high viscosity for stable jetting	PEDOT: PSS[5]-PEO	PET film	3	[22]

1. PEO, poly(ethylene oxide); 2. PCL, (poly-ε-caprolactone); 3. PVDF, (polyvinylidene fluoride); 4. PLGA, poly(lactide-co-glycolide); 5. PEDOT:PSS, Poly(3,4-ethylenedioxythiophene):polystyrene sulfonate

Reference

(1) van de Groep, J.; Spinelli, P.; Polman, A. *Nano Lett.* **2012,** 12 (6), 3138-3144.

(2) Hong, S.; Yeo, J.; Kim, G.; Kim, D.; Lee, H.; Kwon, J.; Lee, H.; Lee, P.; Ko, S. H. *ACS Nano* **2013,** 7 (6), 5024-5031.

(3) Kang, M. G.; Kim, M. S.; Kim, J.; Guo, L. J. *Adv. Mater.* **2008,** 20 (23), 4408-4413.

(4) Jiu, J.; Nogi, M.; Sugahara, T.; Tokuno, T.; Araki, T.; Komoda, N.; Suganuma, K.; Uchida, H.; Shinozaki, K. *J. Mater. Chem.* **2012,** 22 (44), 23561-23567.

(5) Jiang, Z.; Fukuda, K.; Xu, X.; Park, S.; Inoue, D.; Jin, H.; Saito, M.; Osaka, I.; Takimiya, K.; Someya, T. *Adv. Mater.* **2018,** 30 (26), 1707526.

(6) Park, J.; Hwang, J. *J. Phys. D: Appl. Phys.* **2014,** 47 (40), 405102.

(7) Jang, Y.-R.; Chung, W.-H.; Hwang, Y.-T.; Hwang, H.-J.; Kim, S.-H.; Kim, H.-S. *ACS Appl. Mater. Interfaces* **2018,** 10 (28), 24099-24107.

(8) De, S.; Higgins, T. M.; Lyons, P. E.; Doherty, E. M.; Nirmalraj, P. N.; Blau, W. J.; Boland, J. J.; Coleman, J. N. *ACS Nano* **2009,** 3 (7), 1767-1774.

(9) Schneider, J.; Rohner, P.; Thureja, D.; Schmid, M.; Galliker, P.; Poulikakos, D. *Adv. Funct. Mater.* **2016,** 26 (6), 833-840.

(10) Theron, S. A.; Zussman, E.; Yarin, A. L. *Polym.* **2004,** 45 (6), 2017-2030.

(11) Lopez, J.; Pei, A.; Oh, J. Y.; Wang, G.-J. N.; Cui. Y. *J. Am. Chem. Soc.* **2018,** 14 (37), 11735-11744.

(12) Gulez, S. K. H.; Ali Mohsin, M. E.; Shainh, H.; Anis, A.; Pulose, A. M.; Yadav, M. K.; Qua, E. H. P.; Al-Aahrani, S. M. *Polym. Compos.* **2014**, 35 (5), 900-914

(13) Dhapola, P. S.; Singh, P. K.; Bhattacharya, B.; Surana, K.; Mehra, R. M.; Gupta, M.; Singh, A.; Singh, V.; Sahoo, N. G. *Polym.* **2018,** 30 (8), 1002-1008

(14) An, B. W.; Kim, K.; Lee, H.; Kim, S.-Y.; Shim, Y.; Lee, D.-Y.; Song, J. Y.; Park, J.-U. *Adv. Mater.* **2015,** 27 (29), 4322-4328.

(15) Lee, M.; Kim, H.-Y. *Langmuir* **2014,** 30 (5), 1210-1214.

(16) Kim, H.-Y.; Lee, M.; Park, K. J.; Kim, S.; Mahadevan, L. *Nano Lett.* **2010,** 10 (6), 2138-2140.

(17) Hochleitner, G.; Jüngst, T.; Brown, T. D.; Hahn, K.; Moseke, C.; Jakob, F.; Dalton, P. D.; Groll, J. *Biofabrication* **2015,** 7 (3), 035002.

(18) Wunner, F. M.; Wille, M.-L.; Noonan, T. G.; Bas, O.; Dalton, P. D.; De-Juan-Pardo, E. M.; Hutmacher, D. W. *Adv. Mater.* **2018,** 30 (20), 1706570.

(19) Luo, G.; Teh, K. S.; Liu, Y.; Zang, X.; Wen, Z.; Lin, L. *ACS Appl. Mater. Interfaces* **2015,** 7 (50), 27765-27770.

(20) Jordahl, J. H.; Solorio, L.; Sun, H.; Ramcharan, S.; Teeple, C. B.; Haley, H. R.; Lee, K. J.; Eyster, T. W.; Luker, G. D.; Krebsbach, P. H.; Lahann, J. *Adv. Mater.* **2018,** 30 (14), 1707196.

(21) Visser, J.; Melchels, F. P. W.; Jeon, J. E.; van Bussel, E. M.; Kimpton, L. S.; Byrne, H. M.; Dhert, W. J. A.; Dalton, P. D.; Hutmacher, D. W.; Malda, J. *Nat. Commun.* **2015,** 6, 6933.

(22) Chang, J.; He, J.; Lei, Q.; Li, D. *ACS Appl. Mater. Interfaces* **2018,** 10 (22), 19116-19122.